NUMERICAL ANALYSIS OF STATIC LOAD ALLEVIATION FOR TRANSPORT AIRCRAFT

W. Unkelbach*, P. J. González*, B. Herlambang*, M. Ritter†, F. J. Silvestre*

* Technische Universität Berlin, Institute of Aeronautics and Astronautics, Department of Flight Mechanics, Flight Control and Aeroelasticity, Marchstrasse 12, 10587 Berlin, Deutschland

† DLR - Institute of Aeroelasticity, Bunsenstraße 10, 37073 Göttingen, Germany

Abstract

Increasing efficiency in fuel consumption and reducing the environmental impact of aviation can be achieved by load alleviation methods which allow lighter wing structures. This paper presents the implementation and numerical validation of a flight dynamics model for a high aspect ratio aircraft configuration, along with the development of three static load alleviation strategies aimed at reducing the wing root bending moment (RBM) while considering the resulting drag increase. The aerodynamic model was generated using the vortex lattice method via Athena-Vortex-Lattice (AVL) adjusted by computational fluid dynamics (CFD) simulations. Utilizing aerodynamic, geometric, mass and performance data, the flight dynamics simulation was implemented within the modular flight simulation environment of the Department of Flight Mechanics, Flight Control and Aeroelasticity (FMRA). An optimization process with three different optimization targets was implemented and will be described in the paper. The first Pre-Setting (PS) achieves maximum load alleviation. PS 2 penalizes drag increase and performs weighted load alleviation. PS 3 uses only 5 instead of 8 control surfaces. These load alleviation PS, along with the clean configuration, were input into the flight simulation tool and subjected to discrete (1-cos)-shaped gusts with various gradients and amplitudes, as described in the certification specifications CS-25. The configurations were also tested under stochastically distributed turbulence using the von Kármán model of the Matlab/Simulink Aerospace Toolbox. The results were analysed to evaluate the reduction in RBM and the increase in drag. To evaluate the RBM, a routine between the simulation output and AVL was established. The flight dynamics model was further numerically verified through typical characteristic time domain responses of commercial aircraft. Using the evaluation routine, the RBM was calculated through AVL. The analysis focuses on the reduction of RBM and load peaks following different gust encounters. Results indicate that PS 1 offers the maximum load alleviation with all control surfaces, providing the most significant load peak and cycle alleviation but also resulting in a substantial drag increase. The weighted PS 2, designed as a compromise between drag and RBM reduction, shows less reduction than PS 1, but cuts the drag increase significantly, thereby enhancing overall performance. PS 3, which employs fewer control surfaces, proves impractical due to its lower RBM reduction and higher drag increase compared to PS 2, demonstrating the ineffectiveness of using fewer control surfaces.

Keywords

Aircraft Performance; Landing; Approach; Cruise; Flap Deflection; Flight Mechanical Model; Load Alleviation; Transport Aircraft; High-Lift System

NOMENCLATURE

Formelzeichen

α	angle of attack	deg
C	coefficient	-
η	control surface deflection	deg
Ma	Mach number	-

Indices

D	Drag
incompre	incompressible
L	Lift
MFCD	Multi-Functional Control Device
Mr	Root bending moment
P	Pressure
perp	perpendicular
rest	remaing rest

Abbreviations

CC BY 4.0

doi: 10.25967/650052

CAD	Computer-Aided Design
CFD	Computational Fluid Dynamics
CS	Certification Specifications
FMRA	Department of Flight Mechanics, Flight Control and Aeroelasticity
MFCD	Multi-Functional Control Device
MLA	Maneuver Load Alleviation
PS	Pre-Setting
RBM	Root Bending Moment

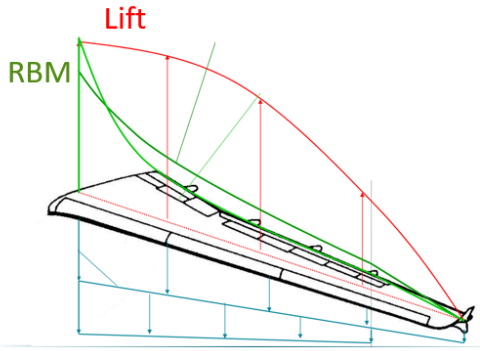

FIG 1. Lift Distribution and RBM over the Wing

1. INTRODUCTION

Recently, there has been an increased interest in reducing aircraft fuel consumption and carbon emissions. There is a global effort to reduce the environmental impact of the entire aviation industry [1]. Aircraft manufacturers, governments, and regulatory bodies adopted the Technology Roadmap for Environmentally Sustainable Aviation in 2008 [2], defining plans and projects to reduce environmental impact in the aviation sector by 2050 to 50 % below what it was in 2005. Also, a reduction of noise emission and fuel consumption are of main interest to increase public acceptance [3]. These policies helped promote the ZEROe program's development by Airbus. This project focuses on designing, developing, and evaluating new and different aircraft concepts with novel configurations and propulsion systems, proposing sustainable aviation fuels and hydrogen as propellant. A common property among these aircraft is, that all seek to reduce fuel consumption by increasing aerodynamic efficiency. One way to reduce induced drag is increasing the aspect ratio which challenges structural design. Particularly the vertical wind component induces additional aerodynamic forces and structural loads. Load alleviation has the goal to minimize these effects and reduce loads through the deflection of control surfaces [4]. This reduces the strain on higher aspect ratio aircraft which reduces structural mass and can save fuel [5]. Previously developed functions for a continuously moving slats and flaps system appeared more promising during approach [6, 7]. The system shall contribute to a smooth approach maneuver and shall allow pilots' full attention on ATC commands without having to think about an efficient flap setting. The second contribution of the system addresses the Flightpath 2050 goals to reduce noise emission and fuel consumption [2, 8]. These concepts are expanded to cruise flight in order to alleviate loads also during the longest phase of the flight [9].
High-lift systems on commercial aircraft are primarily used during take-off and landing to produce sufficient lift at low speeds to compensate for the weight force. During landing, additional drag is required to dissipate the potential and kinetic energy. During cruise flight, partial deflections of the high-lift system are used to reduce the loads on the wing caused by turbulence and maneuvers. New high-lift wings will depend on a reliable load reduction function in order not to lose the aerodynamic advantages of a high-lift wing due to the need to stiffen the structure with additional wing mass [10, 11]. Load alleviation can focus on maneuver loads or gust loads which include turbulence [12].
Within this paper, different methods for gust and turbulence load reduction are compared. The approaches are analyzed and evaluated with regard to their effect on the root bending moment (RBM) of the wings, in particular on the reduction of load peaks. A key idea is to change the lift distribution in order to reduce the lever arm and therefore the bending moment on the wing. This can be graphically seen in Figure 1. Initially, the used flight mechanical model is described, then the methods for reducing load alleviation are mentioned. Finally, these methods are employed and tested in landing and cruise flight in order to compare different strategies and gauge their usefulness.

2. METHODOLOGY

2.1. Flight Mechanical Model

The modular simulation environment ModSig of the FMRA in MATLAB/SIMULINK is used to model the flight mecanics [13]. The simulation is rigid-body with Mach number Ma = 0.3 for landing and Ma = 0.77 for cruise flight. Unlike the landing configuration, the cruise conditions do not allow an incompressible calculation. The Ma is larger than 0.7 and because of that, the Prantl-Glauert transformation is used to correct the aerodynamic derivatives using AVL. The validity of the Prandtl-Glauert transformation depends on the local Ma which takes into consideration the wing sweep. For a swept wing, the perpendicular Mach number is calculated as $Ma_{perp} = Ma \cdot cos(25°) = 0.698$. These derivatives are then used in a Simulink simulation to calculate lift, drag, RBM and other pertinent parameters. The Prandtl-Glauert transformation converts the Prandtl-Glauert equation to the Laplace equation. The Lapalace equation is then solved with the incom-

CC BY 4.0

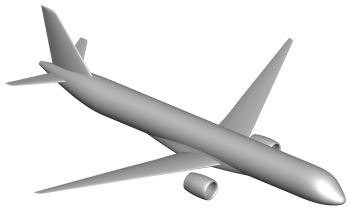

FIG 2. Outer surface of the CFD grid used for the computation of the stability derivatives.

pressible method. For an arbitrary coefficient such as the pressure coefficient the relation between the incompressible and compressible version is defined as $B = c_{P,incompre}/c_P$.

$$\frac{1}{B} = \frac{1}{\sqrt{1 - Ma^2}} \tag{1}$$

B can also be another coefficient like C_L or C_D.

2.2. Longitudinal Stability Derivatives Computed by CFD

A high fidelty CFD based approach was used to compute selected longitudinal stability derivatives of the DLR F25 ULTIMATE-NLF configuration [14]. The objective is to correct especially the lift curve slope from AVL by values of higher accuracy. Compressibility as well as thickness and viscous effects are all accounted for at transonic flight speeds. CFD simulations conducted in other work packages of the ULTIMATE project used a clean wing configuration without engine and pylon [14]. In order to obtain more realistic results for the stability derivatives, a simplified engine, modeled as through-flow nacelle without pylon, was added. The engine and pylon which are included in the CAD model of the clean configuration (as shown in Figure 7) cannot be used at this stage as there is no proper engine model (which would be required for CFD simulations with engine boundary conditions) available for the DLR F25 ULTIMATE-NLF. The outer surface of the CFD model is shown in Figure 2. A hybrid CFD grid of the DLR F25 ULTIMATE-NLF in cruise flight (no control surface deflections) with hexahedral and prismatic boundary layer cells was build, were the cell spacing in the normal direction from surfaces was selected carefully to obtain proper y^+ values at the surfaces and good convergence. For the computation of the derivatives with respect to the angle of attack ($C_{L,\alpha}, C_{M,\alpha}$), steady and quasi-steady CFD simulations were performed for angles of attack from -1 to 3 degrees in steps of one degree. For the derivatives with respect to the pitch rate ($C_{L,q}, C_{M,q}$), the pitch rate was varied from -1 to 1 degrees/s in steps of 0.5 degrees/s. The Mach number is set to 0.77 (cruise flight), the altitude is 10000 m, all other parameters were derived from standard atmosphere conditions. The RANS simulations, which were performed with the DLR TAU-Code [15], use the

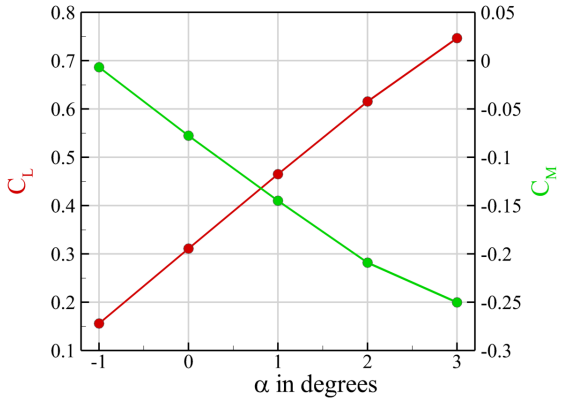

FIG 3. Lift and Moment Coefficients as Function of the Angle of Attack.

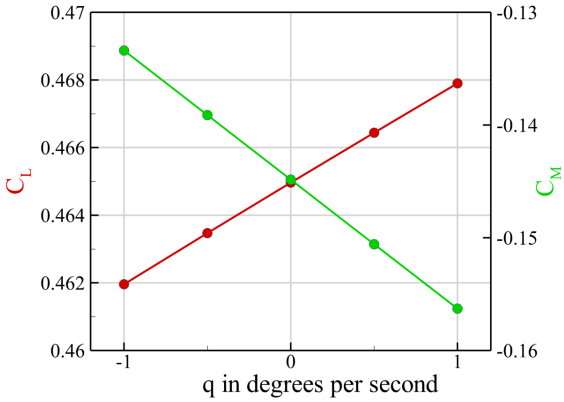

FIG 4. Lift and Moment Coefficients as Function of the Pitch Rate.

SST $k-\omega$ turbulence model, a central scheme with matrix dissipation is used for the convective flux discretization of the mean flow equations. The convective fluxes of the turbulence equations are discretized with a second-order Roe upwind scheme. A local time step is used in combination with an implicit Backward-Euler scheme to accelerate convergence employing an LU-SGS scheme. The *FSDynafly* framework for CFD based flight dynamics and loads analyses was used to compute all data on a high performance cluster [16]. The results in terms of the lift and pitching moment coefficients are shown in Figures 3 and 4 as function of the angle of attack and the pitch rate, respectively.

The values for the angle of attack and the pitch rate were chosen to stay in the linear regime; however, minor nonlinear effects are obtained for an angle of attack from two degrees. A central difference scheme was applied to compute the longitudinal stability derivatives $C_{L,\alpha}$, $C_{M,\alpha}$, $C_{L,q}$, and $C_{M,q}$ from the coefficients. The point of linearization for all derivatives is at one degree angle of attack.

2.3. Workflow

Aerodynamic coefficients are calculated using AVL and CFD as described in Section 2.2. These constants are used in Matlab to create a Simulink Model and perform a trim routine. With variable input data and

CC BY 4.0

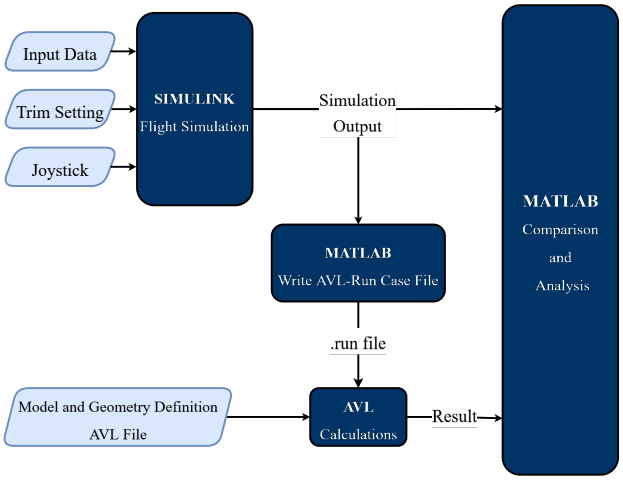

FIG 5. Program Structure

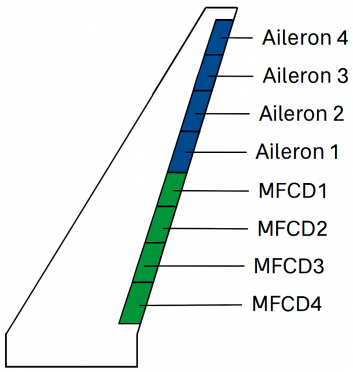

FIG 6. Control Surface Distribution over the Wing

commands the flight simulation is performed which creates output data. This output data can be directly analysed or post-processed via AVL to calulate the bending moment distribution over the wing as well as the RBM. The workflow is shown graphically in Figure 5.

3. LOAD ALLEVIATION METHODS

The main idea of load alleviation is to move the lifting forced more to the center of the wing. The higher the lift far away from the fuselage, the higher the lever arm and resulting bending moment. This is depicted in Figure 1. Different angles of attack for different Pre-Settings (PS) are used, to keep the same total lift coefficient. A central parameter for this loading is the RBM M_r which describes the bending moment at the wing root where it is attached to the fuselage. In order to guarantee the same flight conditions, the lift needs to globally stay the same for any control surface deflection. The outer ailerons could be used to reduce the RBM as well, but are presumed to be used for attitude control. The layout of ailerons and multi-functional control devices (MFCD) can be seen in Figure 6.
Additionally to the MFCD also the inner ailerons are used while aileron-4 is used for attitude control. With help of a coefficient for the load alleviation per control surface deflection C_{Mr} and MFCD deflection η_{MFCD}, the reduction of RBM can be expressed in Eq. 2

Control Surface	max. deflection cruise [°]	max. deflection landing [°]
Flap	/	37.5
MFCD1	±5	±10
MFCD2	±5	±10
MFCD3	±10	±10
MFCD4	±10	±10
Aileron1	±20	±20
Aileron2	±20	±20
Aileron3	±20	±20
Aileron4	±20	±20

TAB 1. Maximum Control Surface Deflection

$$\Delta M_r = \sum_{i=1}^{4} C_{Mr,\mathrm{MFCDi}} \cdot \eta_{\mathrm{MFCDi}} \tag{2}$$

The lift change by control surface deflection is taken into account matrixwise in Eq. 3

$$\begin{bmatrix} C_{L,\mathrm{MFCD1}} & C_{L,\mathrm{MFCD4}} \\ C_{Mr,\mathrm{MFCD1}} & C_{Mr,\mathrm{MFCD4}} \end{bmatrix} \cdot \begin{bmatrix} \eta_{\mathrm{MFCD1}} \\ \eta_{\mathrm{MFCD4}} \end{bmatrix} = \begin{bmatrix} 0 \\ \Delta M_r \end{bmatrix} \tag{3}$$

In case the RBM cannot be reduced sufficiently using MFCD4 or MFCD1 does not provide enough lift to compensate the lift reduction by deflecting MFCD4, MFCD3 and MFCD2 are used. The schematic is employed in Eq. 4.

$$\begin{bmatrix} C_{L,\mathrm{MFCD2}} & C_{L,\mathrm{MFCD3}} \\ C_{Mr,\mathrm{MFCD2}} & C_{Mr,\mathrm{MFCD3}} \end{bmatrix} \cdot \begin{bmatrix} \eta_{\mathrm{MFCD2}} \\ \eta_{\mathrm{MFCD3}} \end{bmatrix} = \begin{bmatrix} 0 \\ \Delta M_{r,rest} \end{bmatrix} \tag{4}$$

The maximum deflections of each control surface are specified in Table 1. Now a cost function is defined to weigh the drag increase by deflecting a control surface in order to reduce the lift. An optimization routine can then find the optimal deflection which reduces RBM and increases drag least.
The cost function for drag and load alleviation in terms of RBM is defined in Eq. 5

$$\begin{aligned} Cost = C_1 * C_{Mr}/mean(C_{Mr})... \\ +C_2 * C_{C_D}/mean(C_{C_D}) \end{aligned} \tag{5}$$

with $C_{1/2} \in [0,1]$. The results an optimization routine using Eq. 5 yields are shown in Tables 2 and 3 for landing and cruise PS respectively. PS 1 only optimizes RBM with $C_2 = 0$ while PS 3 does not take the use of MFCD3, MFCD4 and aileron-1 into account.
Aileron-4 is solely used for attitude control and has no static deflection for load alleviation purposes. The deflected control surfaces exemplary for cruise flight are depicted in Figures 7, 8 and 9 for no deflection, PS

CC BY 4.0

Control Surface	PS 1 [°]	PS 2 [°]	PS 3 [°]
Flap	37.5	37.5	37.5
MFCD1	10	-9.11	-5.6
MFCD2	1.45	-9	-10
MFCD3	-10	-9	0
MFCD4	-10	-9.33	0
Aileron1	-20	-2	0
Aileron2	-20	-2.88	-20
Aileron3	-20	-2	-20

TAB 2. Landing PS

Control Surface	PS 1 [°]	PS 2 [°]
Flap	0	0
MFCD1	5	5
MFCD2	5	2.8
MFCD3	10	3.3
MFCD4	-5.6	-1.1
Aileron1	-2.2	-2.2
Aileron2	-20	-6.7
Aileron3	-20	-6.7

TAB 3. Cruise PS

1 and PS 2 respectively. Table 4 shows the reductions of RBM and the impact of the drag.

4. PERFORMANCE ANALYSIS

In the following the results for the landing and then the cruise load alleviation methods are discussed. First 1-cosine-gusts were implemented and analyzed. Afterwards the methods described in Section 3 were compared using stochastical turbulence. For this the von-Kármán model was used which only depends on the scale length. The intensity is defined in [17] according to altitude. In the following subsections the results for landing are shown in detail for a gust response and the abbreviated results are shown for cruise flight under stochastic turbulence. The for cruise omitted plots are analogous to the ones in Subsection 4.1.

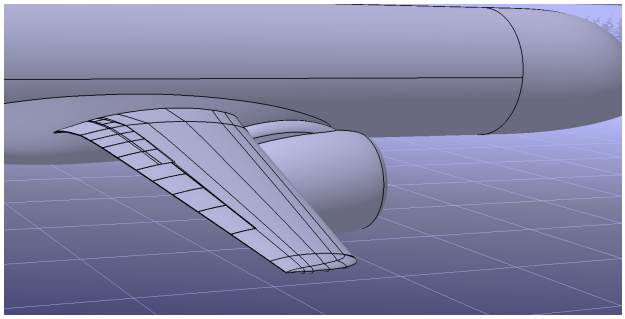

FIG 7. CAD Model of Clean Configuration

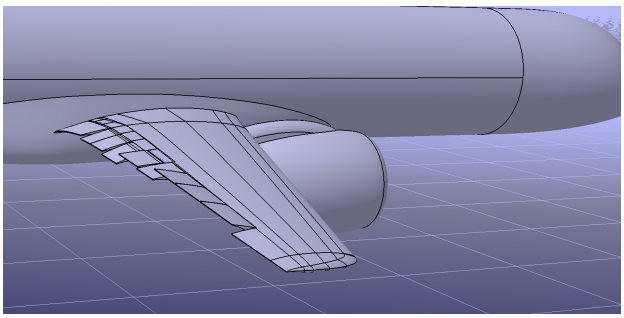

FIG 8. CAD Model of PS 1

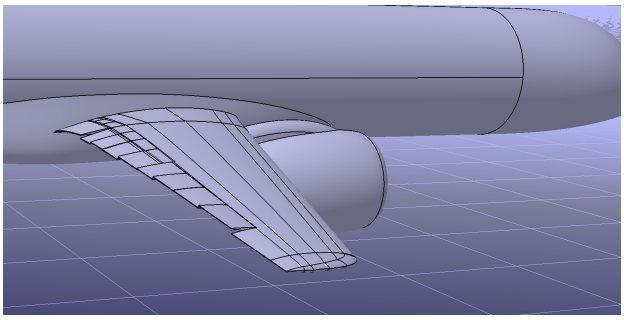

FIG 9. CAD Model of PS 2

4.1. Landing

In the landing scenario the load alleviation methods are compared as depicted in Figures 10 to 13. A change in angle of attack $\Delta\alpha = \alpha_{trim} - \alpha$ is depicted in Figure 10 for a representative time of 20 s. The trim values of the angle of attack are $\alpha_{trim}(clean) = 7.3\ °$, $\alpha_{trim}(PS\ 1) = 8.3\ °$, $\alpha_{trim}(PS\ 2) = 9.6\ °$ and $\alpha_{trim}(PS\ 3) = 8.7\ °$. This is due to the fact that in order to match the flight condition, the angle of attack varies for different control surface deflections. The lift coefficients are compared in Figure 11. This leads to a similar trend for the RBM, which can be seen in Figure 12. With a reduction in RBM comes an increase in drag due to the control surface deflection. The drag coefficient is shown in Figure 13. The values of RBM reduction and drag increase are compared in Table 4. Evidently PS 1 leads to the highest RBM reduction as well as the highest drag increase. PS 3 which uses fewer control surfaces increases the drag significantly but fails to lower the RBM effectively. PS 2 shows a good RBM reduction with minor drag increase. Depending on the situation PS 1 and PS 2 can be useful in a landing scenario. For a landing case additional drag can be advantageous, e.g. when a reduction in speed is desirable. This makes PS 1 more attractive in landing scenarios. For cruise flight additional drag is expensive and unwanted.

	PS 1	PS 2	PS 3
RBM reduction	36.97 %	22.98 %	15.62 %
C_D increase	6.05 %	3.73 %	1.88 %

TAB 4. Landing Flight Results

CC BY 4.0

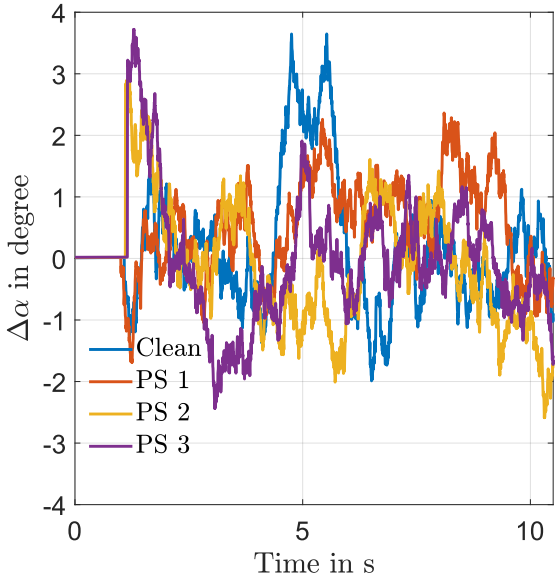

FIG 10. Angle of Attack Deviation for Landing Flight

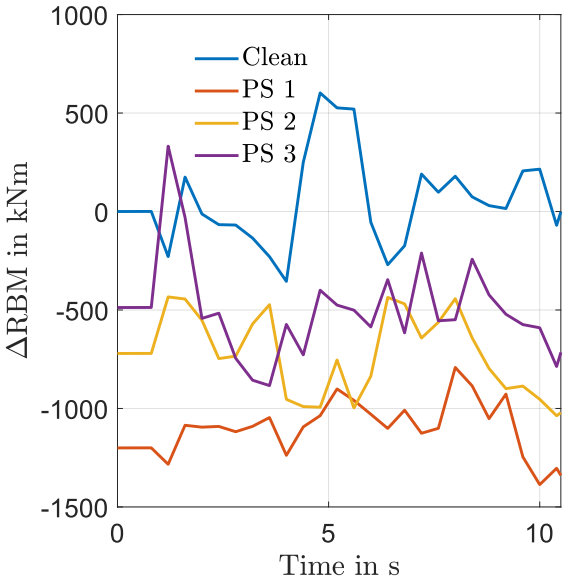

FIG 12. RBM for Landing Flight

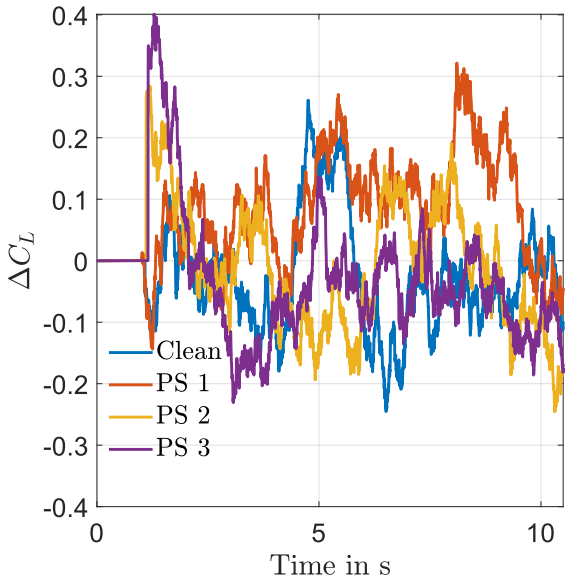

FIG 11. Lift Coefficient for Landing Flight

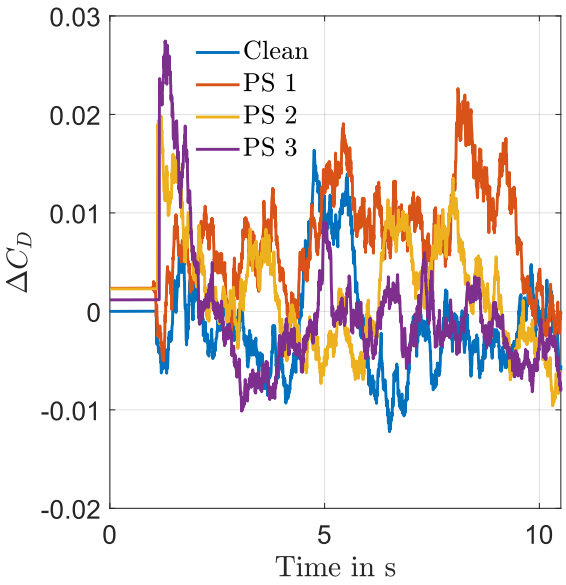

FIG 13. Drag Coefficient for Landing Flight

CC BY 4.0

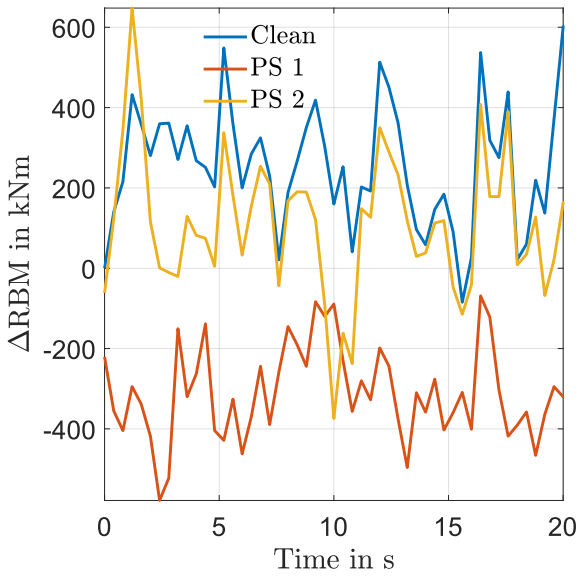

FIG 14. RBM for Cruise Flight

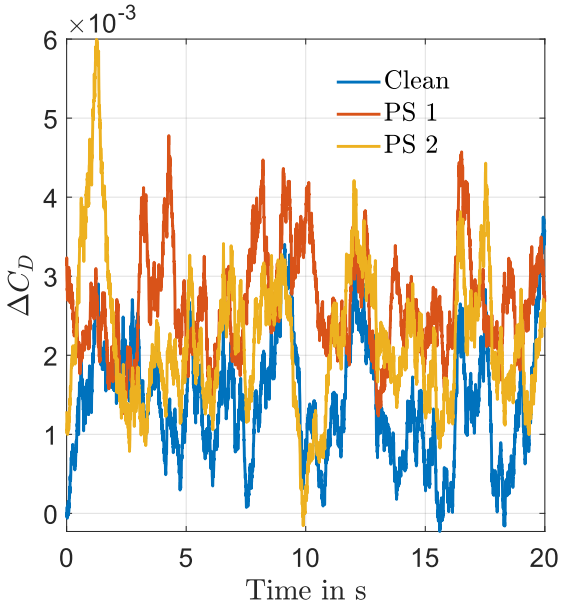

FIG 15. Drag Coefficient for Cruise Flight

	PS 1	PS 2
RBM reduction	15.29 %	3.78 %
C_D increase	4.12 %	2.62 %

TAB 5. Cruise Flight Results

Due to its initial poor performance in comparison with PS 2, for cruise flight PS 3 which makes use of only some of the control surfaces was discarded. The results in Table 4 indicate however a good performance of PS 3. A version for cruise flight is therefore desirable and could be implemented as future work. A lower number of control surfaces needs less actuation which is additionally advantageous.

4.2. Cruise

Similar to the landing results also the RBM reduction and drag are plotted in Figures 14 and 15. The highest RBM reduction is achieved by PS 1 which also creates the most drag. PS 2 only causes a minor drag increase, but alleviates the wing loading significantly. This can be seen in Table 5. In a cruise case where fuel is an essential consideration PS 2 has a better efficiency, achieving half the RBM reduction with only a third of the drag increase in comparison to PS 1. In situations with heavy turbulence PS 1 might be viable for a short period of time. Also ride comfort is a topic that can be investigated in the future, here other advantages could also justify a higher fuel consumption. Active load alleviation for maneuvers can provide the same RBM reduction and be a better alternative for cruise flight.

5. CONCLUSION

Results indicate that PS 1 offers the maximum load alleviation with all control surfaces, providing the most significant load peak and cycle alleviation but also resulting in a substantial drag increase. The weighted PS 2, designed as a compromise between drag and RBM reduction, shows less reduction than PS 1, but cuts the drag increase significantly, thereby enhancing overall performance. PS 3, which employs fewer control surfaces, proves impractical due to its lower RBM reduction and higher drag increase compared to PS 2, demonstrating the ineffectiveness of using fewer control surfaces. For landing, where drag increase is helpful, PS 1 is most promising as a load alleviation method which can be employed during descent. For cruise flight PS 2 provides the best efficiency in terms of fuel while also reducing the loads.

5.1. Outlook

Preliminary results show that an active controller is able to provide better maneuver load alleviation and can also reduce gust loads better than a static load alleviation device. For turbulence also due to actuation energy costs the static load alleviation methods are a good option. In future work the different load alleviation methods are tested in a flight simulator, so that inputs of real pilots can evaluate the method's feasibility in an as realistic as possible environment. Then a final evaluation of load alleviation methods will be delivered. An iteration of PS 3 for cruise flight appears promising due to lower actuation demands.

Acknowledgement

The work presented in this paper was funded by the German Federal Ministry for Economic Affairs and Energy (BMWE) due to resolution of the German Federal Parliament within the scope of the LuFo VI-2 compound project ULTIMATE (grant number 20A2101A). The authors gratefully acknowledge this support.

CC BY 4.0

Contact address:

wilhelm.unkelbach@tu-berlin.de

References

[1] Air Transportation Action Group. Aviation benefits beyond borders, 2014. [Retrieved: 03-Jun-2025]. https://aviationbenefits.org/media/26786/ATAG__AviationBenefits2014_FULL_LowRes.pdf.

[2] Airbus. Zeroe: Towards the world's first zero-emission commercial aircraft, 2020. [Retrieved: 03-Jun-2025]. https://www.airbus.com/en/innovation/zero-emission/hydrogen/zeroe.

[3] G. Topham. Anti-aviation sentiment shared across europe, say uk campaigners, 2012. [Retrieved: 10-Jul-2025]. https://www.theguardian.com/business/2012/oct/21/anti-aviation-europe-campaigners.

[4] R. König and K.-U. Hahn. Load alleviation and ride smoothing investigations using attas. In *Proceedings of the 17th ICAS Congress*, pages 1379–1393, Oberpfaffenhofen, 1990. Deutsches Zentrum für Luft- und Raumfahrt.

[5] V. Handojo. Investigation of load alleviation in aircraft pre-design and its influence on structural mass and fatigue. *Aerospace Science and Technology*, 122:107405, 2022.

[6] P. Stukenborg and R. Luckner. Evaluating the influence of continuous flap settings on the take-off performance of an airliner using flight simulation. *CEAS Aeronautical Journal*, 2018. DOI: 10.1007/s13272-018-0315-2.

[7] P. Stukenborg and R. Luckner. Evaluating the influence of continuous flap settings on the approach performance of an airliner using flight simulation. 2019. Presented at DLRK 2018. DOI: 10.25967/480161.

[8] European Union. Flightpath 2050: Europe's vision for aviation maintaining global leadership & serving society's needs, 2011. [Retrieved: 10-Jul-2025]. DOI: 10.2777/50266, https://ec.europa.eu/transport/sites/transport/files/modes/air/doc/flightpath2050.pdf.

[9] H. Höhnlinger, H. Zimmermann, O. Sensburg, and J. Becker. Structural aspects of active control technology. In *Active Control Technology: Applications and Lessons Learned*, pages 18–1–18–25. Neuilly-Sur-Seine, 1994.

[10] A. Mancini, M. Roelofs, and R. Vos. The effect of maneuver load alleviation strategies on aircraft performance indicators. In *AIAA Aviation 2019 Forum*, pages 1–17, Dallas, 2019. American Institute of Aeronautics and Astronautics Inc.

[11] F. Großmann and M. Pusch. Lpv-reglerentwurf zur böenlastabminderung am flexiblen flugzeug. In *Deutscher Luft- und Raumfahrtkongress 2016*, pages 1–9, Braunschweig, 2016. Deutsche Gesellschaft für Luft- und Raumfahrt - Lilienthal-Oberth e.V.

[12] T. Kier and G. Looye. Unifying manoeuvre and gust loads analysis models. Technical Report IFASD-2009-106, German Aerospace Center, Institute of Robotics and Mechatronics, Oberpfaffenhofen, 2009.

[13] A. Quesada, P. González, G. Barbosa, G. Stavorinus, and F. Silvestre. Influence of nonlinear aerodynamic effects on high aspect ratio aircraft model. In *IFASD 2024-International Forum on Aeroelasticity and Structural Dynamics, Madrid, Spain*, 2024.

[14] Martin Schmalz, Markus Raimund Ritter, and Michael Fehrs. Numerical analysis of boundary-layer transition on a high-aspect ratio backward-swept laminar wing considering different mass cases. In *24. DGLR-Fachsymposium der STAB*, Regensburg, November 2024.

[15] D. Schwamborn, T. Gerhold, and R. Heinrich. The dlr tau-code: Recent applications in research and industry. In *ECCOMAS Conference*, Delft, Netherlands, 2006.

[16] Markus Raimund Ritter, Mathias Stefan Roeser, and Stefan Görtz. Multi-axis maneuver simulation for system identification of flexible transport aircraft by high-fidelity methods. In *32nd Congress of the International Council of the Aeronautical Sciences, ICAS 2021*, September 2021.

[17] U.S. Department of Defense. MIL-F-8785C: Flying qualities of piloted airplanes, 1980. Military Standard MIL-F-8785C.

CC BY 4.0